Effects of finite-system size in nonlinear optical systems: A quantum many-body approach to parametric oscillation

Oliver Veits and Michael Fleischhauer
Sektion Physik, Ludwig-Maximilians-Universität München, Theresienstraße 37, D-80333 München, Germany
(Received 4 October 1996)

We analyze the influence of system-size effects on the quantum properties of a degenerate parametric oscillator below, at, and above the classical threshold using a Green's-function approach. The many-body technique permits a systematic analysis of finite-size corrections to standard linearization results. In particular we study a ''semiquantum'' limit, where even above threshold only few photons are in the subharmonic mode while the pump mode is highly populated and behaves quasiclassically. Substantial deviations from classical and linearization predictions are found. We show that the depletion of the pump mode is rather strong and the threshold of parametric oscillation is shifted to higher pump strength, when the subharmonic system is small. [S1050-2947(97)07803-7]

PACS number(s): 42.50.Lc, 42.50.Dv, 42.65.Ky, 42.50.Ct

I. INTRODUCTION

The phase transition of a degenerate optical parametric oscillator (OPO) is an extensively studied subject in quantum optics since one of the quadrature components of the down-converted field can display a complete suppression of quantum fluctuations at the critical point [1], which has a variety of potential applications in low-noise communication and high-sensitivity measurements. From a theoretical point of view this phase transition is interesting because it is dominated by quantum fluctuations, which are increasingly important, when the so-called system size becomes small. The analysis of system-size effects and their influence on the fluctuations and correlation times in the vicinity of the critical point are therefore essential for the understanding of the phase transition. The frequently used linearization approximation [2] implicitly assumes a thermodynamic limit and cannot be used to study finite-size effects [3]. Furthermore, the inherent small-noise assumption breaks down at the critical point. A consistent description of the quantum dynamics thus requires an approach which does not resort to the standard linearizations.

Analytical solutions of the nonlinear problem are known only in the limit of a fast decaying pump mode where an adiabatic elimination of this mode is possible. The reduced Fokker-Planck equation for the subharmonic mode fulfills potential conditions and can be solved analytically in steady state [4–7]. Information about correlation times and scaling properties in the adiabatic limit has recently been obtained by Kinsler and Drummond, who mapped the dynamical equations of the degenerate parametric oscillator onto the cubic stochastic process [8].

A very promising approach to the general case, which goes beyond the standard linearization, has been introduced by Mertens, Kennedy, and Swain [9–11] and modified by Plimak and Walls [12]. They applied nonequilibrium many-body techniques to calculate finite-size corrections close to the classical threshold. In this approach no adiabatic elimination is required. However the convergence of the self-consistent calculation scheme in Refs. [9–11] breaks down in the immediate vicinity of the critical point, since it uses ill-behaved linearized Green's functions as a starting point. Thus the scaling properties at the classical threshold could not be analyzed.

In the present paper we follow the idea of Mertens, Kennedy, and Swain and apply many-body Green's-function techniques to the OPO. Different from their approach, however, we use as a starting point in the self-consistent calculation scheme expressions from a mean-field approximation, which we developed in Ref. [13]. In this approach the lowest order contributions are well behaved also at the critical point, since the backaction of fluctuations on the mean coherent amplitudes is taken into account. We are thus able to calculate average values and fluctuations also at the classical threshold and can study the scaling of fluctuations and correlation times with the system size at this point.

The Green's-function (GF) formalism is an approach to calculate ordered correlation functions. It involves a truncation of a hierarchy of equations, which is done here by an expansion of the so-called vertex function [14]. This expansion is applicable for a large range of parameters and breaks down only in the strong quantum limit of very small photon numbers in both the pump and the subharmonic mode. Since this limit can easily be treated by a numerical evaluation of the Fock-state density matrix equations, it shall not be considered here. On the other hand, there are two system-size parameters in the OPO corresponding to the two modes, and pronounced quantum effects are to be expected if only one of these parameters becomes small. We will show that the lowest-order term in the vertex expansion, the bare-vertex approximation, works very well when the system-size of the pump mode is kept large. However, at the same time the system size of the subharmonic mode may be chosen rather small. It is thus possible to study the ''semiquantum'' limit of a small-sized subharmonic and quasiclassical pump mode in which substantial deviations from the classical and linearization approaches are found. This ''semi-quantum'' limit is achieved when the cavity-loss rate of the pump mode γ_2 is small compared to that of the subharmonic mode γ_1, a situation complementary to the adiabatic limit studied in [4–8,12].

 © 1997 The American Physical Society

We will show that the range of validity of the bare-vertex approximation can go far beyond the classical threshold when $\gamma=\gamma_2/\gamma_1$ is small and still works reasonably well at threshold even for values of γ of the order of unity. In the limit of γ going to zero the bare-vertex approximation reduces to the mean-field approximation discussed in Ref. [13], which can be solved analytically under stationary conditions.

Above the classical threshold the bare-vertex solution undergos a trifurcation. One solution follows the mean-field result (vanishing subharmonic amplitude), while the other solutions approach the above-threshold classical behavior with a broken symmetry. The trifurcation point, which may be considered as the renormalized threshold of parametric oscillation, is shifted more and more above the classical threshold, when the system size is reduced.

Our paper is organized as follows. In Sec. II we describe the model and compare the mean-field with the standard linearization approach. We also study the scaling properties of fluctuations and correlation times at the classical threshold in the mean-field approximation. In Sec. III we give an introduction into nonequilibrium many-body techniques for three-boson interactions and establish some simple notation. The reader familiar with nonequilibrium Green's functions may skip this part. In Sec. IV we specialize to the case of a degenerate optical parametic oscillator, assuming first a vanishing mean amplitude of the subharmonic mode (i.e., not allowing for symmetry breaking). Here we analyze the fluctuation properties below, at, and to a certain extent above the classical threshold within the bare-vertex approximation. Dyson equations for normal and anomalous Green's functions (correlation functions) are derived and solved numerically in a self-consistent way. Squeezing and antisqueezing spectra are calculated and the dependence on pump strength and system size are discussed. The range of validity of the bare-vertex approach is analyzed by numerical estimating lowest-order corrections to the bare vertex in a second part of Sec. IV. Finally we discuss the bare-vertex solutions above the classical threshold relaxing the condition $\langle a_1\rangle=0$ (i.e., allowing for symmetry breaking). Section V gives a summary and an outlook.

II. CLASSICAL BEHAVIOR, SMALL-NOISE, AND MEAN-FIELD APPROXIMATIONS

The degenerate OPO is a system of two coupled cavity quasimodes of frequency ω and 2ω. The high-frequency mode with photon annihilation and creation operators a_2 and $a_2^\dagger$ is driven by an external classical field. The cavity contains a nonlinear $\chi^{(2)}$ crystal which splits a pump photon in two subharmonic photons. The corresponding interaction Hamiltonian reads

$$V_{\mathrm{OPO}}=i\hbar\frac{K}{2}(a_2a_1^{\dagger 2}-\mathrm{H.c.})+i\hbar\epsilon(a_2-a_2^\dagger), \tag{1}$$

where K is a real and positive coupling constant, ϵ is the pumping rate which we choose real, and a_1 and $a_1^\dagger$ are the annihilation and creation operators of the subharmonic mode. The damping rates of the two modes due to cavity losses are denoted by γ_1 and γ_2. The dynamics of the system can be described by Heisenberg-Langevin equations

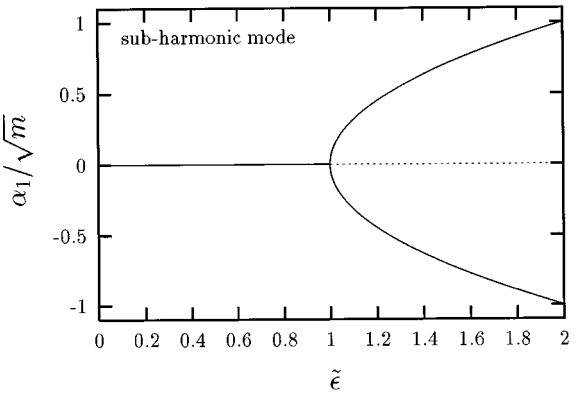

FIG. 1. Classical behavior of the scaled subharmonic amplitude $\tilde{\alpha}_1$ in a degenerate parametric oscillator as a function of the scaled pump strength $\tilde{\epsilon}$. At the classical threshold $\tilde{\epsilon}=1$ the subharmonic mode undergoes a pitchfork bifurcation.

$$\frac{d}{dt}a_1=-\gamma_1a_1+Ka_2a_1^\dagger+\sqrt{2\gamma_1}F_1(t), \tag{2}$$

$$\frac{d}{dt}a_2=-\gamma_2a_2+\epsilon-\frac{K}{2}a_1^2+\sqrt{2\gamma_2}F_2(t), \tag{3}$$

where F_1 and F_2 are δ-correlated fluctuation forces. Due to the invariance of the equations with respect to a sign change of a_1, the subharmonic mode has in the classical limit either a vanishing amplitude or displays a bistable behavior. A transition between the two cases occurs, when the external pump rate ϵ reaches the critical value $\epsilon_{\mathrm{th}}=\gamma_1\gamma_2/K$. Here the classical stationary solutions of Eqs. (2) and (3) show the well-known pitchfork bifurcation of the subharmonic mode shown in Fig. 1. The bifurcation point is the classical threshold of parametric oscillation. Below threshold the subharmonic amplitude is zero and the pump-mode amplitude increases linearly with ϵ. Above threshold the pump mode stays constant and all energy is transferred into the subharmonic mode.

In the standard linearization approach [15], the steady-state quantum behavior of the system is analyzed by assuming small fluctuations around the classical amplitudes and disregarding higher order noise contributions. One of the eigenvalues of the linearized equations vanishes at the classical threshold indicating a critical behavior of the subharmonic mode and the breakdown of the small-noise assumption. The linearized theory is therefore not a useful starting point for a systematic derivation of corrections. Instead we here use the mean-field approach introduced by us in Ref. [13] as a lowest-order approximation. A brief outline of the mean-field approach will be given in the following.

To characterize the scale of the quantum fluctuations in the two modes we first introduce so-called system-size parameters. One is the photon number of the pump mode at threshold in the classical limit

$$n_{\mathrm{th}}=\frac{\gamma_1^2}{K^2} \tag{4}$$

and the other one the slope of the subharmonic photon number above threshold

$$m=\frac{2\gamma_1\gamma_2}{K^2}=2\gamma n_{\rm th}. \tag{5}$$

Normalizing the field operators to these scales,

$$\tilde{a}_1=a_1/\sqrt{m}, \tag{6}$$

$$\tilde{a}_2=a_2/\sqrt{n_{\rm th}}, \tag{7}$$

the pump rate to the threshold value $\tilde{\epsilon}=\epsilon/(\gamma_1\gamma_2/K)$, and measuring time in units of γ_1^{-1} we find the scaled Heisenberg-Langevin equations

$$\frac{d}{d\tau}\tilde{a}_1=-\tilde{a}_1+\tilde{a}_2\tilde{a}_1^{+}+\sqrt{\frac{2}{m}}F_1(\tau), \tag{8}$$

$$\frac{1}{\gamma}\frac{d}{d\tau}\tilde{a}_2=-\tilde{a}_2+\tilde{\epsilon}-\tilde{a}_1^2+\sqrt{\frac{2}{n_{\rm th}}}F_2(\gamma\tau), \tag{9}$$

where $\gamma\equiv\gamma_2/\gamma_1$. From these equations we easily see that the steady-state values for the amplitudes obey

$$\langle\tilde{a}_1\rangle=\langle\tilde{a}_2\tilde{a}_1^{\dagger}\rangle, \tag{10}$$

$$\langle\tilde{a}_2\rangle=\tilde{\epsilon}-\langle\tilde{a}_1^2\rangle. \tag{11}$$

In the standard linearization approach all second- and higher-order contributions in the fluctuations of the field modes around their mean amplitudes are neglected, which corresponds to

$$(\tilde{a}_2-\langle\tilde{a}_2\rangle)(\tilde{a}_1^{\dagger}-\langle\tilde{a}_1^{\dagger}\rangle)\approx 0, \tag{12}$$

$$(\tilde{a}_1-\langle\tilde{a}_1\rangle)^2\approx 0. \tag{13}$$

This approximation leads to a diverging subharmonic photon number at threshold, since it ignores the depletion of the pump mode due to energy transfer into subharmonic fluctuations. However, we replace here the operator expressions on the left-hand side of Eqs. (12) and (13) by their average value in the spirit of a mean-field or Hartree approximation. This amounts to the replacement

$$\tilde{a}_2\tilde{a}_1^{\dagger}\approx\langle\langle\tilde{a}_2\tilde{a}_1^{\dagger}\rangle\rangle+\langle\tilde{a}_2\rangle\tilde{a}_1^{\dagger}+\tilde{a}_2\langle\tilde{a}_1^{\dagger}\rangle-\langle\tilde{a}_2\rangle\langle\tilde{a}_1^{\dagger}\rangle, \tag{14}$$

$$\tilde{a}_1^2\approx\langle\langle\tilde{a}_1^2\rangle\rangle+2\langle\tilde{a}_1\rangle\tilde{a}_1-\langle\tilde{a}_1\rangle^2, \tag{15}$$

where $\langle\langle xy\rangle\rangle\equiv\langle xy\rangle-\langle x\rangle\langle y\rangle$.

Since the Heisenberg-Langevin equations (8) and (9) become linear in the operators when the mean-field approximation (14) and (15) is applied, we can easily calculate the steady-state values of $\langle\langle\tilde{a}_2\tilde{a}_1^{\dagger}\rangle\rangle$ and $\langle\langle\tilde{a}_1^2\rangle\rangle$ as a functional of $\tilde{\alpha}_1\equiv\langle\tilde{a}_1\rangle$, $\tilde{\alpha}_2\equiv\langle\tilde{a}_2\rangle$, and $1/m=[\tilde{a}_1,\tilde{a}_1^{\dagger}]$. We find

$$\langle\langle\tilde{a}_2\tilde{a}_1^{\dagger}\rangle\rangle=\frac{\tilde{\alpha}_1\tilde{\alpha}_2^2\gamma(2+2\tilde{\alpha}_1^2+\gamma)}{(\tilde{\alpha}_2^2-4\tilde{\alpha}_1^2-4\tilde{\alpha}_1^4-1)(1-\tilde{\alpha}_2^2+2\gamma+\gamma^2)m}, \tag{16}$$

$$\langle\langle\tilde{a}_1^2\rangle\rangle=-\frac{\tilde{\alpha}_2}{2}\frac{1+4\tilde{\alpha}_1^2+4\tilde{\alpha}_1^4-\tilde{\alpha}_2^2+2\gamma+6\tilde{\alpha}_1^2\gamma+4\tilde{\alpha}_1^4\gamma+\gamma^2+2\tilde{\alpha}_1^2\gamma^2}{(\tilde{\alpha}_2^2-4\tilde{\alpha}_1^2-4\tilde{\alpha}_1^4-1)(1-\tilde{\alpha}_2^2+2\gamma+\gamma^2)m}, \tag{17}$$

where we have made use of the fact that $\tilde{\alpha}_1$ and $\tilde{\alpha}_2$ are real if ϵ is real and positive. Substituting these results back into Eqs. (10) and (11) leads to a set of nonlinear algebraic equations for $\langle\tilde{a}_1\rangle$ and $\langle\tilde{a}_2\rangle$. For $1/m=0$, i.e., in the thermodynamic limit of an infinite system size, $\langle\langle\tilde{a}_2\tilde{a}_1^{\dagger}\rangle\rangle$ and $\langle\langle\tilde{a}_1^2\rangle\rangle$ vanish except at the critical point and the solutions for $\langle\tilde{a}_1\rangle$ and $\langle\tilde{a}_2\rangle$ are the classical ones with a bistable result above threshold. For any finite value of m, however, only the solution

$$\langle\tilde{a}_1\rangle=\langle\tilde{a}_2\tilde{a}_1^{\dagger}\rangle=0 \tag{18}$$

survives. That is in the mean-field approximation the correlation between the subharmonic and pump amplitude vanishes and there are no bistable solutions. Under this condition we find

$$\langle\tilde{a}_1^2\rangle=\frac{\langle\tilde{a}_2\rangle}{2m(1-|\langle\tilde{a}_2\rangle|^2)} \tag{19}$$

and

$$\langle\tilde{a}_1^{\dagger}\tilde{a}_1\rangle=\frac{|\langle\tilde{a}_2\rangle|^2}{2m(1-|\langle\tilde{a}_2\rangle|^2)}. \tag{20}$$

Similarly the steady-state pump-field amplitude follows from the third-order nonlinear equation

$$\langle\tilde{a}_2\rangle=\tilde{\epsilon}-\frac{\langle\tilde{a}_2\rangle}{2m(1-|\langle\tilde{a}_2\rangle|^2)}, \tag{21}$$

which results from substituting Eq. (19) into Eq. (11). Only one of the three roots of Eq. (21) obeys $|\langle\tilde{a}_2\rangle|<1$, a condition which is required for obtaining positive photon number in the subharmonic mode [see Eq. (20)]. In Fig. 2 we have plotted this solution as a function of the scaled pump rate $\tilde{\epsilon}$ for different values of m. In the ''semiquantum'' limit of small m values a substantial deviation from the classical result can be recognized. The mean-field theory does not show any symmetry breaking in the subharmonic mode, i.e., $\langle\tilde{a}_1\rangle$ stays zero also above threshold. Nevertheless the stable classical solution $\langle\tilde{a}_2\rangle=1$ is approached above threshold for in-

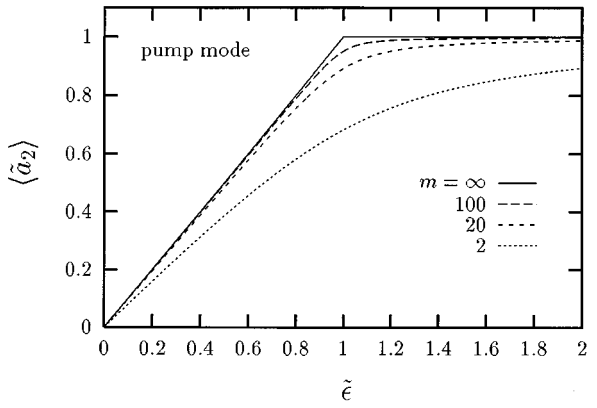

FIG. 2. Scaled mean amplitude of pump mode $\langle\tilde{a}_2\rangle$ as function of scaled pump strength $\tilde{\epsilon}$ according to mean-field equation (21) for different values of system-size parameter m.

creasing system size m. Similarly the mean photon number of the subharmonic mode $\langle n_1\rangle$ approaches the classical value as shown in Fig. 3.

The linear Langevin equation for the subharmonic mode in mean-field approximation is identical to that of the standard linearization approach [15] except that the classical value $\tilde{\alpha}_2^{\mathrm{cl}}$ has to be replaced by the mean-field solution $\langle\tilde{a}_2\rangle$ of Eq. (21),

$$\frac{d}{d\tau}\tilde{a}_1=-\tilde{a}_1+\langle\tilde{a}_2\rangle\tilde{a}_1^{\dagger}+\sqrt{\frac{2}{m}}F_1. \tag{22}$$

Thus the squeezing spectra of the two quadrature components

$$x_1(t)=\frac{1}{2}[a_1(t)+a_1^{\dagger}(t)], \tag{23}$$

$$p_1(t)=\frac{1}{2i}[a_1(t)-a_1^{\dagger}(t)] \tag{24}$$

are given by the known Lorentzians

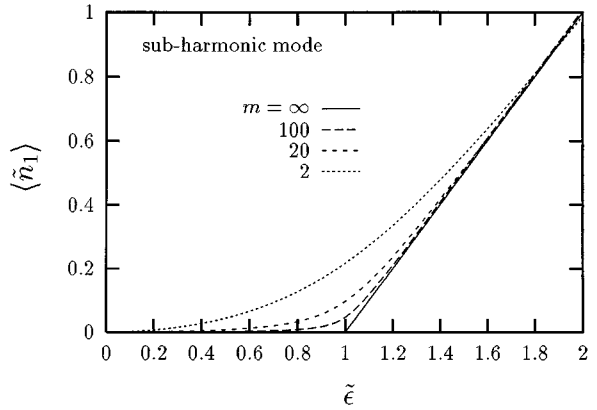

FIG. 3. Scaled subharmonic photon number as a function of pump strength in mean-field approximation according to Eq. (20) for different values of m.

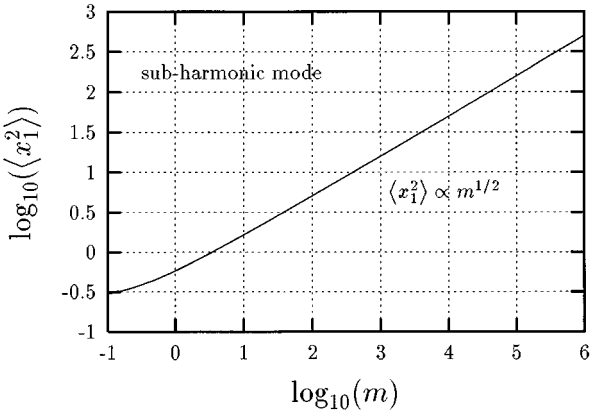

FIG. 4. System-size scaling of intracavity antisqueezed fluctuations in mean-field approximation.

$$S_{\pm}(\omega)=\pm\frac{\langle\tilde{a}_2\rangle}{\omega^2/\gamma_1^2+(1\mp\langle\tilde{a}_2\rangle)^2}. \tag{25}$$

Here the indices + and − correspond to the ''coordinate'' and ''momentum'' quadrature of the field, respectively.

Since $\langle\tilde{a}_2\rangle$ remains smaller than unity, the subharmonic fluctuations do not diverge in contrast to the standard linearization result. We can therefore study the scale of the fluctuations in the squeezed and antisqueezed quadrature at the classical threshold $\tilde{\epsilon}=1$. The squeezed (antisqueezed) fluctuations in the output spectrum at $\omega=0$ scale with m^{-1} (m). The intracavity fluctuations of the antisqueezed component x_1 as shown in Fig. 4 as well as the subharmonic photon number scale with $m^{1/2}$. While in the linearization approach there is a critical slow down of the fluctuations in the antisqueezed quadrature, they again remain finite in the mean-field approximation. We find that the decay rate of the squeezed fluctuations becomes independent on the system size and that of the antisqueezed fluctuations vanishes with $m^{-1/2}$. This is shown in Fig. 5. These results are consistent with the adiabatic results of Wolinski and Carmichael [7] and Kinsler and Drummond [8].

Since $\langle\tilde{a}_2\rangle$ monotonically approaches unity for increasing pump rate, the maximum amount of squeezing in the p_1 component or, respectively, the maximum fluctuation in x_1 are attained only for an infinite pump rate. Clearly the valid-

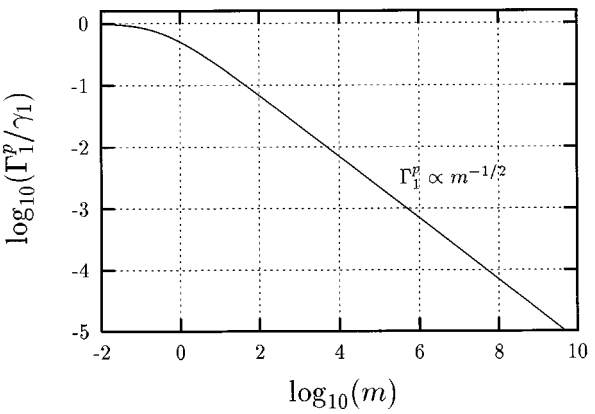

FIG. 5. System-size scaling of correlation decay of antisqueezed quadrature in mean-field approximation.

ity of the mean-field approximation breaks down much earlier. Nevertheless, we can conclude that the point of maximum fluctuations is shifted to higher pump strength values due to finite-size quantum corrections.

The mean-field approach breaks down, when either the fluctuations of the pump mode or fluctuations of $\tilde{a}_1^2$ around its average value $\langle \tilde{a}_1^2 \rangle$ become important. As we will show later on, rather small values of γ are required for an accurate description of the threshold behavior by the mean-field approach. Nevertheless, also for larger values of γ the approach gives a well behaved zeroth-order approximation and is therefore a useful starting point for further considerations. Furthermore, it yields the correct system-size scaling of the fluctuations at the classical threshold.

III. QUANTUM MANY-BODY APPROACH

In the present section we will give a short introduction into nonequilibrium many-body techniques [14] applied to problems in nonlinear quantum optics. We also establish some notations which will be helpful further on.

A. Green's functions, Feynman graphs, and perturbation theory

The aim of the many-body approach is to derive closed sets of equations for n-point Green's functions (or n-time correlation functions), which have the generic form

$$\langle T^{-1}[A_H(t_1)\cdots]T[\cdots A_H(t_m)]\rangle. \tag{26}$$

Here A_H denotes an operator in the Heisenberg picture corresponding to some field mode, T is the time-ordering operator, and $\langle\cdots\rangle$ means $\mathrm{Tr}\{\rho_0\cdots\}$, where ρ_0 is the density operator at $t=-\infty$, which is assumed to fulfill the conditions for the application of Wick's theorem [14]. It should be noted that it is sufficient to consider time-ordered correlation functions of the form given in Eq. (26), since these are the only measurable quantities of the field [16]. All relevant statistical information can be derived from the Green's functions and in most cases only a few are actually needed.

In the case of a nonlinear interaction it is not possible to obtain a closed set of equations in an exact way, but rather an infinite hierarchy of equations arises. To find appropriate approximations it is useful to first separate the solvable linear part of the problem. For this we introduce an interaction picture, in which the field operators evolve according to the free Hamitonian plus the reservoir interactions describing cavity losses. The corresponding operators in the interaction picture are denoted by A. Any time-ordered correlation function of operators A_H of the type given in Eq. (26) can then be expressed by interaction picture operators with the help of the time-evolution operator

$$S=T\exp\left\{-\frac{i}{\hbar}\int_{-\infty}^{\infty}dt' V(t')\right\}. \tag{27}$$

$$\langle T^{-1}[A_H(t_1)\cdots]T[\cdots A_H(t_m)]\rangle = \langle T^{-1}[S^{-1}A(t_1)\cdots]T[S\cdots A(t_m)]\rangle. \tag{28}$$

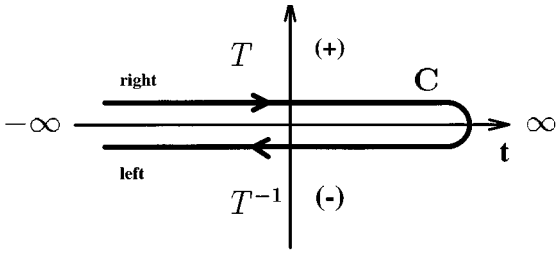

FIG. 6. Schwinger-Keldysh time contour C. To each physical time correspond two contour times, on upper $(+)$ or lower branch $(-)$ depending on whether it appears in a causal or anticausal time ordered expression.

To simplify the notation it is useful at this point to introduce the so-called Schwinger-Keldysh time contour C [17] indicated in Fig. 6 and a corresponding time-ordering operator T_C which is identical to T on the upper branch of the contour and to T^{-1} on the lower one. If we furthermore define that T_C orders all operators on the lower branch to the left of those on the upper branch, Eq. (28) can be expressed with a single time-ordering and evolution operator on C:

$$\langle T_C[A_H(t_1^{(-)})\cdots A_H(t_m^{(+)})]\rangle = \langle T_C[S_C A(t_1^{(-)})\cdots A(t_m^{(+)})]\rangle \tag{29}$$

and

$$S_C = T_C\exp\left\{-\frac{i}{\hbar}\int_C d\check{t}\,V(\check{t})\right\}, \tag{30}$$

where $\check{t}$ denotes a time argument on the contour C and the superscripts $(\pm)$ specify the branch.

We denote the exact Green's functions on the Schwinger-Keldysh contour by

$$D_i(\check{t}_i)\equiv\langle T_C S_C A_i(\check{t}_i)\rangle, \tag{31}$$

$$D_{ij}(\check{t}_i,\check{t}_j)\equiv\langle T_C S_C A_i(\check{t}_i)A_j(\check{t}_j)\rangle - D_i(\check{t}_i)D_j(\check{t}_j), \tag{32}$$

and the free Green's functions D_i^0 and D_{ij}^0 by the same expressions without S_C. The subscript $i\in\{m^+,m\}$ indicates that A_i creates or annihilates a photon of mode m. We note that the definition (32) contains also so-called anomalous Green's functions with two annihilation or creation operators, which are needed to describe quadrature squeezing. Sometimes we will find it useful to work with physical times, in which case we explicitly denote the contour branch by indices:

$$D_{ij}^{\alpha\beta}(t_i,t_j)\equiv\langle T_C S_C A_i(t_i^\alpha)A_j(t_j^\beta)\rangle - D_i^\alpha(t_i)D_j^\beta(t_j), \tag{33}$$

where $\alpha,\beta\in\{+,-\}$.

At this point let us discuss some symmetry properties of the Green's functions, as they help to substantially reduce the calculational effort. It is immediately obvious from Eq. (32) that

$$D_{ij}(\check{t}_i,\check{t}_j)\equiv D_{ji}(\check{t}_j,\check{t}_i). \tag{34}$$

Complex conjugation of a Green's function turns an annihilation operator into a creation operator and vice versa. In addition, the ordering is reversed. This is done by switching the time contour labels $+\leftrightarrow-$,

$$(D_{ij}^{\alpha\beta}(t_i,t_j))^* \equiv D_{i^+,j^+}^{-\alpha-\beta}(t_i,t_j). \tag{35}$$

The action of the time-ordering operator can be written as

$$TA(t_1)B(t_2)=\theta(t_1-t_2)A(t_1)B(t_2)+\theta(t_2-t_1)B(t_2)A(t_1)$$

and similar for the antitime-ordering operator. With respect to the two-point Green's functions this leads to the identities

$$D_{ij}^{++}+D_{ij}^{--}=D_{ij}^{+-}+D_{ij}^{-+}, \tag{36}$$

$$D_{ij}^{++}-D_{ij}^{--}=2\,\mathrm{sgn}(t_i-t_j)(D_{ij}^{-+}-D_{ij}^{+-}). \tag{37}$$

Let us now consider as a generic example for a nonlinear interaction a three-boson process with coherent driving. In Einstein-notation, where one has to sum over all pairs of indices, the interaction Hamiltonian reads

$$V(\check{t})=i\hbar\,\frac{1}{3!}v_{klm}A_k(\check{t})A_l(\check{t})A_m(\check{t})+i\hbar\,\epsilon_k A_k(\check{t}). \tag{38}$$

In order to calculate the exact two-point Green's function for such a process, we start with a perturbation approach. We expand S_C in $D_{ij}\equiv\langle T_C S_C A_i A_j\rangle - D_i D_j$ in powers of the elementary vertices v_{klm} and ϵ_k,

$$\begin{aligned}S_C=1&+\int_C d\check{t}\,\epsilon_k A_k(\check{t})+\frac{1}{3!}\int_C d\check{t}\;v_{klm}T_C[A_k(\check{t})A_l(\check{t})A_m(\check{t})]+\frac{1}{2!}\int\int_C d\check{t}d\check{t}'\,\epsilon_k\epsilon_l T_C[A_k(\check{t})A_l(\check{t}')]\\&+\frac{1}{(3!)^2}\frac{1}{2!}\int\int_C d\check{t}d\check{t}'v_{klm}v_{npq}T_C[A_k(\check{t})A_l(\check{t})A_m(\check{t})A_n(\check{t}')A_p(\check{t}')A_q(\check{t}')]\\&+\frac{1}{3!}\int\int_C d\check{t}d\check{t}'\,\epsilon_k v_{lmn}T_C[A_k(\check{t})A_l(\check{t}')A_m(\check{t}')A_n(\check{t}')]+\cdots.\end{aligned} \tag{39}$$

Applying Wick's theorem, which also holds for interaction-picture operators that include the reservoir coupling, we can now express the exact correlation functions in terms of interaction-picture correlation functions,

$$D_i(\check{1})=\int_C d\check{2}\,\epsilon_k D_{ik}^0(\check{1},\check{2})+\frac{1}{2!}\int_C d\check{2}D_{ik}^0(\check{1},\check{2})v_{klm}D_{lm}^0(\check{2},\check{2})+\cdots, \tag{40}$$

$$\begin{aligned}D_{ij}(\check{1},\check{1}')=&D_{ij}^0(\check{1},\check{1}')+\int\int_C d\check{2}d\check{3}D_{ik}^0(\check{1},\check{2})v_{klm}D_{ln}^0(\check{2},\check{3})\left[\epsilon_n+\frac{1}{2!}v_{npq}D_{pq}^0(\check{3},\check{3})\right]D_{mj}^0(\check{3},\check{1}')\\&+\frac{1}{2!}\int\int_C d\check{2}d\check{3}D_{ik}^0(\check{1},\check{2})v_{klm}D_{ln}^0(\check{2},\check{3})D_{mp}^0(\check{2},\check{3})v_{npq}D_{qj}^0(\check{3},\check{1}')+\cdots.\end{aligned} \tag{41}$$

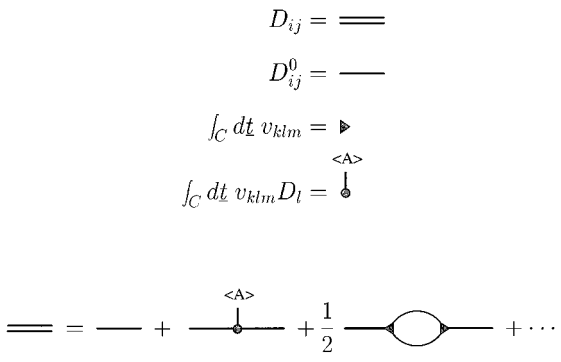

FIG. 7. Graphical representation of exact (double line) and free (single line) one-photon Green's functions. Also shown are the linear and nonlinear vertices (at which an integration over the contour C has to be performed) and the graphical representation of the first terms in a perturbation expansion of the exact GF D in terms of the free GF D^0.

Here we have introduced $\check{1},\check{2},\ldots$ to abbreviate time arguments.

For a very convenient graphical notation of the involved equations we use Feynman-diagrams. As shown in Fig. 7, we use a single or double line to represent a free or exact two-point Green's function. In addition there are two-end and three-end vertices denoted by circles and triangles, respectively, at which an integration over the whole Schwinger-Keldysh contour has to be performed. Using this notation the perturbation expansion (41) can be given the simple graphical representation also shown in Fig. 7.

In order to obtain a nonperturbative result for the exact two-point Green's functions one has to sum up the terms in

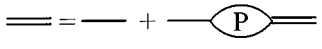

FIG. 8. Graphical representation of the Dyson equation with formal self-energies. The self-energies represent all diagram blocks that cannot be separated in two parts by cutting a single GF line.

the series expansion. In the general case this is not possible and one must resort to a partial summation of the series which takes into account the most dominant terms. This will be explained in the next subsection.

B. Self-energy and Dyson equation

A formal summation of all terms in the perturbation expansion of an exact Green's function can be obtained by introducing the so-called self-energy. The self-energy P is formally the sum of all diagram blocks with two external vertices, which cannot be separated by cutting a single GF line. With these definitions one obtains a closed set of Dyson equations [14] for the two-point Green's functions:

$$D_{ij}(\check{1},\check{1}') = D^0_{ij}(\check{1},\check{1}') + \int\int_C d\check{2}d\check{3} D^0_{ik}(\check{1},\check{2}) \times P_{kl}(\check{2},\check{3}) D_{lj}(\check{3},\check{1}'). \quad (42)$$

Figure 8 gives a graphical representation of this equation. Transforming Eq. (42) into physical times we find

$$D^{\alpha\beta}_{ij}(1,1') = D^{0\,\alpha\beta}_{ij}(1,1') + \int\int_{-\infty}^{\infty} d2d3 D^{0\,\alpha\gamma}_{ik}(1,2) \times \gamma P^{\gamma\delta}_{kl}(2,3)\,\delta D^{\delta\beta}_{lj}(3,1'), \quad (43)$$

where the factors γ and δ $(=\pm 1)$ come from the fact that the integration direction is reversed on the lower branch of the time contour. In a compact notation, where the Green's functions and the self-energies become 2×2 matrices denoted by $\mathbf{D}_{ij}$ and $\mathbf{P}_{ij}$, we have

$$\mathbf{D}_{ij}(1,1') = \mathbf{D}^0_{ij}(1,1') + \int\int_{-\infty}^{\infty} d2d3 \mathbf{D}^0_{ik}(1,2)\mathbf{P}_{kl}(2,3) \times \mathbf{D}_{lj}(3,1'), \quad (44)$$

where we have incorporated the sign factors in the definition of the self-energy matrix $\mathbf{P}_{kl}$.

Under stationary conditions the Green's functions and self-energies depend only on the difference of the (physical) time arguments. A Fourier transformation then turns the integral equation into an algebraic one: Defining $X(\omega) = \int d\tau X(t+\tau,t)\exp\{-i\omega\tau\}$ we arrive at

$$\mathbf{D}_{ij}(\omega) = \mathbf{D}^0_{ij}(\omega) + \mathbf{D}^0_{ik}(\omega)\mathbf{P}_{kl}(\omega)\mathbf{D}_{lj}(\omega). \quad (45)$$

Equation (45) can be solved and the exact Green's functions can be expressed in terms of free Green's functions and self-energies. The introduction of self-energies, however, does only formally solve the problem. One has yet to find good approximations for these quantities. An established procedure to obtain an approximate closed expression for self-energies in many-body theory is the vertex expansion outlined in the next subsection.

C. Vertex expansion and self-energies in bare-vertex approximation

In systems with nonvanishing mean amplitudes of fields, the self-energies P_{ij} can formally be decomposed into two

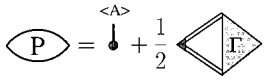

FIG. 9. Representation of self-energy P in terms of the linear mean-field vertex, exact Green's functions, and vertex functions Γ.

contributions. One of them contains the mean amplitude and the other one can be written as a product of two exact Green's functions (GF) and a so-called vertex function $\Gamma_{ijk}(1,2,3)$, which depends on three time arguments [14]. In the language of Feynman graphs, Γ represents all diagram blocks which cannot be separated into three parts by cutting two GF lines:

$$P_{ij}(\check{1},\check{2}) = v_{ijk}D_k(\check{1})\,\delta(\check{1},\check{2}) + \frac{1}{2!}\int\int_C d\check{3}d\check{4} v_{ikl} \times D_{km}(\check{1},\check{3})D_{ln}(\check{1},\check{4})\Gamma_{mnj}(\check{3},\check{4},\check{2}). \quad (46)$$

A graphical illustration of Eq. (46) is given in Fig. 9. The vertex functions Γ_{ijk} can be expanded in powers of the coupling strength v and exact Green's functions. The first terms of such an expansion are shown in Fig. 10. Taking into account only the first term results in the so-called bare-vertex approximation [10], in which we have

$$\Gamma^{(1)}_{ijk}(\check{1},\check{2},\check{3}) = v_{ijk}\delta(\check{1},\check{2})\,\delta(\check{2},\check{3}). \quad (47)$$

This truncation of the vertex-expansion leads to a closed set of Dyson equations for the two-point Green's functions, with the self-energies

$$P_{ij}(\check{1},\check{2}) \approx v_{ijk}D_k(\check{1})\,\delta(\check{1},\check{2}) + \frac{1}{2!}v_{ikl}D_{km}(\check{1},\check{2})D_{ln}(\check{1},\check{2})v_{mnj}. \quad (48)$$

Under stationary conditions we thus have

$$P^{\alpha\beta}_{ij}(\omega) = \alpha\delta_{\alpha\beta}v_{ijk}D^{\alpha}_k + \frac{1}{4\pi}\int d\omega'\,\alpha\beta v_{ikl}D^{\alpha\beta}_{km}(\omega') \times D^{\alpha\beta}_{ln}(\omega-\omega')v_{mnj}. \quad (49)$$

In order to test the validity of the bare-vertex approximation one can estimate the contributions from the next-order term in the vertex expansion to the self-energies. The second-order term in the vertex expansion reads

$$\Gamma^{(2)}_{ijk}(\check{1},\check{2},\check{3}) = v_{ilm}v_{jnp}D_{ln}(\check{1},\check{2})D_{mq}(\check{1},\check{3})D_{pr}(\check{2},\check{3})v_{qrk}. \quad (50)$$

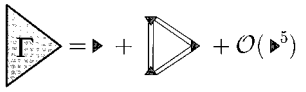

FIG. 10. Expansion of vertex function Γ in powers of coupling strength K and exact Green's functions. The bare-vertex approximation corresponds to a truncation of the expansion after the first term.

This term gives rise to the second-order contribution in the self-energies,

$$P_{ij}^{(2)}(\check{1},\check{2})=\frac{1}{2!}\int\int_C d\check{3}d\check{4}v_{ikl}D_{km}(\check{1},\check{3})D_{lq}(\check{1},\check{4})v_{mnp}\times D_{nr}(\check{3},\check{4})v_{qrs}D_{pt}(\check{3},\check{2})D_{su}(\check{4},\check{2})v_{tuj}. \quad (51)$$

IV. MANY-BODY APPROACH TO THE OPO

We now apply the many-body techniques outlined in the preceding section to the degenerate optical parametric oscillator with the interaction Hamiltonian given by

$$V_{\mathrm{OPO}}=i\hbar\frac{K}{2}(a_2a_1^{\dagger 2}-\mathrm{H.c.})+i\hbar\epsilon(a_2-a_2^{\dagger}). \quad (52)$$

A comparision with the definition of v_{klm} in Eq. (38) gives us $v_{1^+1^+2}=v_{1^+21^+}=v_{21^+1^+}=K$ and $v_{112^+}=v_{12^+1}=v_{2^+11}=-K$ and all others are zero. The statistical properties of the two modes are determined by the normal Green's functions $D_{1^+1}=\langle T_C S_C a_1^+ a_1\rangle$ and $D_{2^+2}=\langle T_C S_C a_2^{\dagger}a_2\rangle$, and the anomalous Green's functions $D_{11}=\langle T_C S_C a_1 a_1\rangle$, $D_{22}=\langle T_C S_C a_2 a_2\rangle$ and their conjugates.

Due to the symmetry of the problem, the mean amplitude of the subharmonic mode $\langle\tilde{a}_1\rangle$ must vanish in steady state. Correspondingly according to Eq. (10) all mixed-type Green's functions $D_{12^+}=\langle T_C S_C a_1 a_2^{\dagger}\rangle$, etc., vanish. However, being an approximation to the exact dynamics, the bare-vertex equations may have multistable solutions above threshold. Therefore also $\langle\tilde{a}_1\rangle\neq 0$ is possible, which corresponds to a symmetry braking. In the first part of this section we discuss the case $\langle\tilde{a}_1\rangle\equiv 0$, i.e., we do not allow for symmetry breaking. In the second part we lift this restriction and show that the bare-vertex solutions become multistable for a critical pump strength $\epsilon_{cr}>\epsilon_{\mathrm{thr}}$, following either $\langle\tilde{a}_1\rangle=0$ or approaching the classical bistable behavior $\langle\tilde{a}_1\rangle=\pm\tilde{\alpha}_1^{\mathrm{cl}}$.

A. The stationary OPO in bare-vertex approximation and $\langle\tilde{a}_1\rangle\equiv 0$

Specifying the discussion of the preceding section to the interaction Hamiltonian of the optical parametric oscillator given in Eq. (52), and noting that $\langle\tilde{a}_1\rangle\equiv 0$ implies that all mixed-type Green's functions vanish, we find the following set of stationary Dyson-equations in Fourier space:

$$\mathbf{D}_{1^+1}(\omega)=\mathbf{D}_{1^+1}^0(\omega)+\mathbf{D}_{1^+1}^0(\omega)\mathbf{P}_{11}(\omega)\mathbf{D}_{11}(\omega)+\mathbf{D}_{1^+1}^0(\omega)\mathbf{P}_{11^+}(\omega)\mathbf{D}_{1^+1}(\omega), \quad (53)$$

$$\mathbf{D}_{11}(\omega)=\mathbf{D}_{11^+}^0(\omega)\mathbf{P}_{1^+1}(\omega)\mathbf{D}_{11}(\omega)+\mathbf{D}_{11^+}^0(\omega)\mathbf{P}_{1^+1^+}(\omega)\mathbf{D}_{1^+1}(\omega), \quad (54)$$

and analogously for mode 2. The self-energies read in bare-vertex approximation

$$P_{11}^{\alpha\beta}(\omega)=K\alpha\delta_{\alpha\beta}\langle a_2\rangle+\frac{K^2}{2\pi}\alpha\beta\int d\omega' D_{11}^{\alpha\beta}(\omega')\times D_{2^+2^+}^{\alpha\beta}(\omega-\omega'), \quad (55)$$

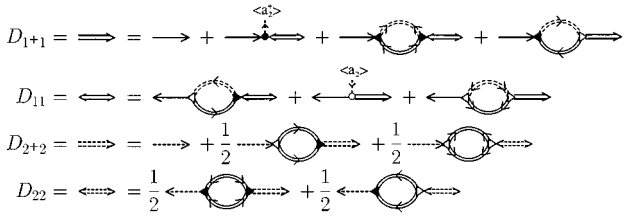

FIG. 11. Graphical representation of Dyson equations for OPO in bare-vertex approximation and $\langle\tilde{a}_1\rangle=0$.

$$P_{1^+1^+}^{\alpha\beta}(\omega)=-K\alpha\delta_{\alpha\beta}\langle a_2^{\dagger}\rangle+\frac{K^2}{2\pi}\alpha\beta\int d\omega' D_{1^+1^+}^{\alpha\beta}(\omega')D_{22}^{\alpha\beta}(\omega-\omega'), \quad (56)$$

$$P_{1^+1}^{\alpha\beta}(\omega)=-\frac{K^2}{2\pi}\alpha\delta_{\alpha\beta}\int d\omega' D_{1^+1}^{\alpha\beta}(\omega')D_{22^+}^{\alpha\beta}(\omega-\omega'), \quad (57)$$

$$P_{22}^{\alpha\beta}(\omega)=\frac{K^2}{4\pi}\alpha\beta\int d\omega' D_{1^+1^+}^{\alpha\beta}(\omega')D_{1^+1^+}^{\alpha\beta}(\omega-\omega'), \quad (58)$$

$$P_{2^+2}^{\alpha\beta}(\omega)=-\frac{K^2}{4\pi}\alpha\beta\int d\omega' D_{11^+}^{\alpha\beta}(\omega')D_{11^+}^{\alpha\beta}(\omega-\omega'). \quad (59)$$

The mean amplitude of the pump mode follows from Eq. (11):

$$\langle a_2\rangle=\frac{\epsilon}{\gamma_2}-\frac{K}{2\gamma_2}\int_{-\infty}^{\infty}\frac{d\omega}{2\pi}D_{11}^{-+}(\omega). \quad (60)$$

A graphical representation of the Dyson equations is given in Fig. 11. Here again single lines are used for free Green's functions and double lines for exact ones. Dashed lines represent the pump mode and full lines the subharmonic mode.

The solution of the Dyson equations (53)–(59) reduces to the solution of

$$\mathbf{D}_{i^+i}(\omega)^{-1}=\mathbf{D}_{i^+i}^0(\omega)^{-1}-\mathbf{P}_{ii^+}^{\mathrm{eff}}(\omega) \quad (61)$$

with the effective self-energies,

$$\mathbf{P}_{ii^+}^{\mathrm{eff}}(\omega)=\mathbf{P}_{ii^+}(\omega)+\mathbf{P}_{ii}(\omega)[\mathbf{1}-\mathbf{D}_{ii^+}^0(\omega)\mathbf{P}_{i^+i}(\omega)]^{-1}\mathbf{D}_{ii^+}^0(\omega)\times\mathbf{P}_{i^+i^+}(\omega). \quad (62)$$

All other Green's functions follow from $\mathbf{D}_{i^+i}$. Since the self-energies contain convolution integrals of exact Green's functions, Eqs. (53)–(59) need to be solved in a self-consistent way by a numerical iteration scheme. Important for the convergence of such a scheme are good initial approximations to the Green's functions and mode amplitudes. Mertens, Kennedy, and Swain used in their analysis expressions from the linearized theory. Since the Green's functions obtained from a linearized theory diverge close to the classical thresh-

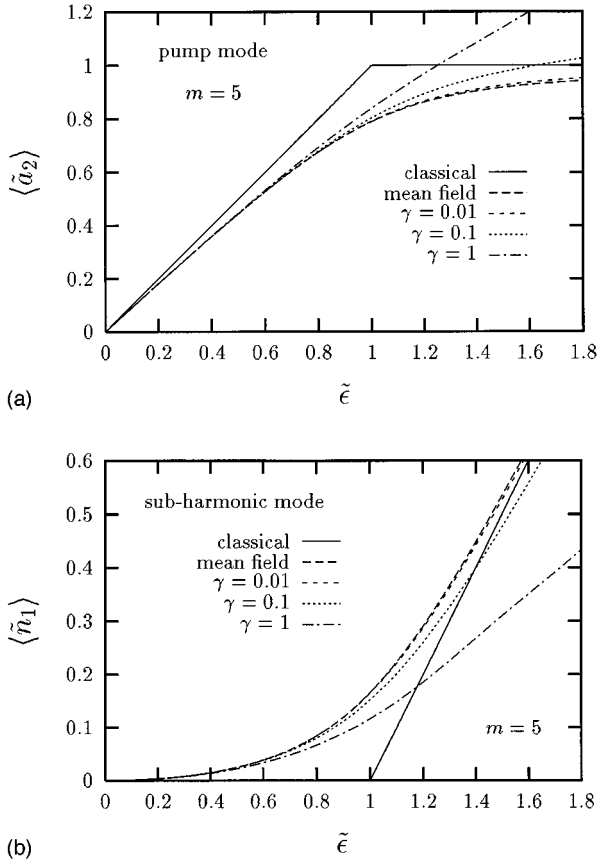

FIG. 12. Pump-mode amplitude (a) and subharmonic photon number (b) as a function of pump rate from bare-vertex and mean-field approximations for a system-size parameter $m=5$.

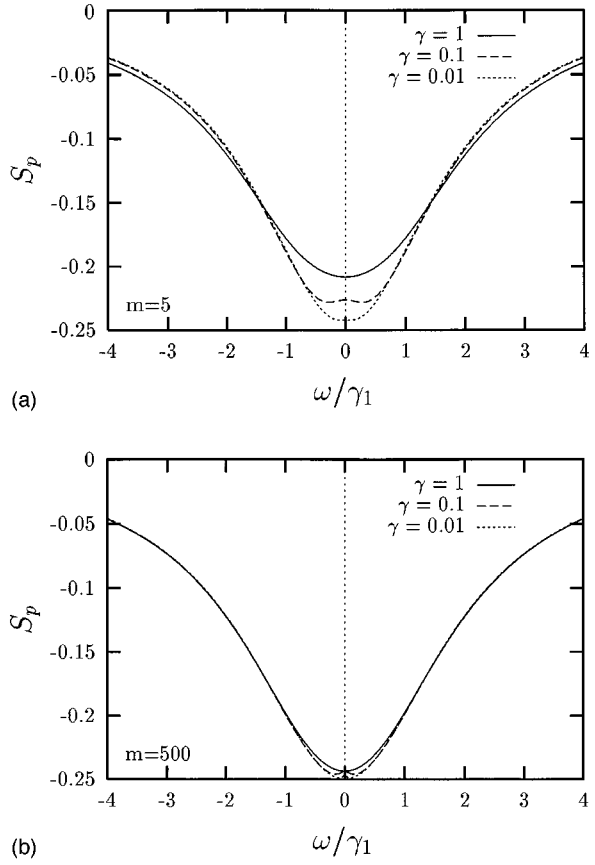

FIG. 13. Squeezing spectra from bare-vertex approach at classical threshold for $m=5$ and $m=500$.

old, this method failed when the critical point was approached. We use here expressions from the mean-field approach of Sec. II for the initial value of the mean pump amplitude $\langle \tilde{a}_2 \rangle$ ($\langle \tilde{a}_1 \rangle = 0$ in mean-field approximation) and for the zeroth-order Green's functions. In order to improve the convergence of the iteration scheme, we did not use the Dyson equations in the form given in Eqs. (53)–(59), but a modified version with the generic structure:

$$\mathbf{D}_{k+1} = \eta[(\mathbf{D}^0)^{-1} - \mathbf{P}_k]^{-1} + (1-\eta)[(\mathbf{D}^0)^{-1} - \mathbf{P}_{k-1}]^{-1}, \tag{63}$$

where k is the iteration index and η is some appropriately chosen parameter between 0 and 1. After each step we obtain updated expressions for the Green's functions from the solution of Eq. (63) and updated expressions for the pump-mode amplitude from Eq. (60). In this way we were able to achieve convergence at and also above the classicial threshold.

In Fig. 12 we have plotted the coherent amplitude of the pump mode and the subharmonic photon number as a function of the pumping strength (all in scaled units) for different values of $\gamma = \gamma_2/\gamma_1$, i.e., for different ratios of pump and subharmonic decay rates. For pump rates below or in the vicinity of the classical threshold the bare-vertex solutions agree with the mean-field results. If the pump rate is further increased, the bare-vertex results start to depart from the mean-field solutions. One recognizes agreement over a relatively large range of pump values for smaller values of γ. As we will show in the next subsection, this can easily be understood when we compare the mean-field and bare-vertex contributions to the self-energies.

In Fig. 13 we have shown our numeric results for the squeezing spectrum of the subharmonic mode at the classical threshold $\tilde{\epsilon}=1$ for a small and a large system size of the subharmonic mode ($m=5$ and $m=500$) and different values of γ (correponding to different system sizes of the pump mode). For a small system size of both modes (m small, γ large) the squeezing at the classical threshold is substantially reduced due to finite-size effects. However, a reduction of squeezing is already present, if only the subharmonic system is small. Correspondingly, the antisqueezed fluctuations do not diverge as opposed to the linearization result. One further recognizes that the one-loop contributions may lead to a double-peak structure of the squeezing spectrum already at the classical threshold.

Figure 14 shows the squeezing spectra for $m=5$ and different values of γ slightly below, at, and slightly above the classical threshold. Corresponding plots for $m=50$ are shown in Fig. 15. One recognizes that for small system sizes of both modes (m small, $\gamma=1$) a maximum in the output squeezing spectrum is achieved below the classical threshold. Decreasing γ, i.e., increasing the pump-mode system size, shifts the point of maximum squeezing to higher pump values. Moreover, the double-peak structure known from the above-threshold linearization [15] becomes visible for $\tilde{\epsilon}=1.2$, despite the fact that there is no symmetry breaking in

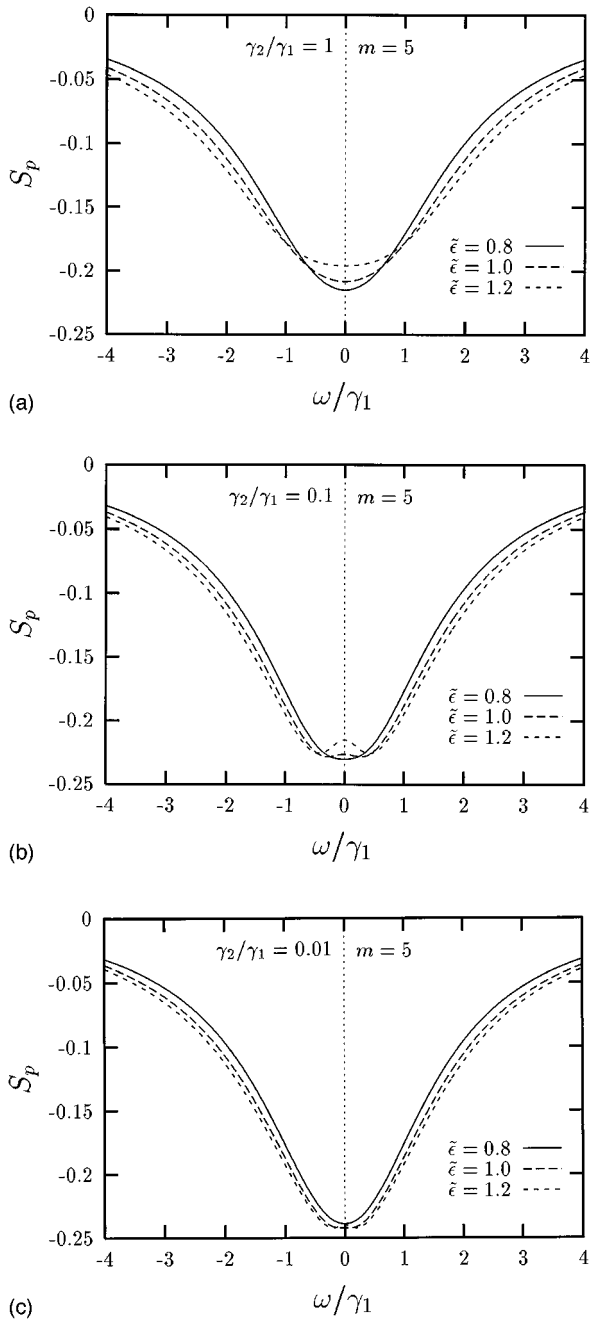

FIG. 14. Squeezing spectra for $m=5$ and $\gamma=0.1$ below ($\tilde{\epsilon}=0.8$), at ($\tilde{\epsilon}=1$), and slightly above the classical threshold ($\tilde{\epsilon}=1.2$).

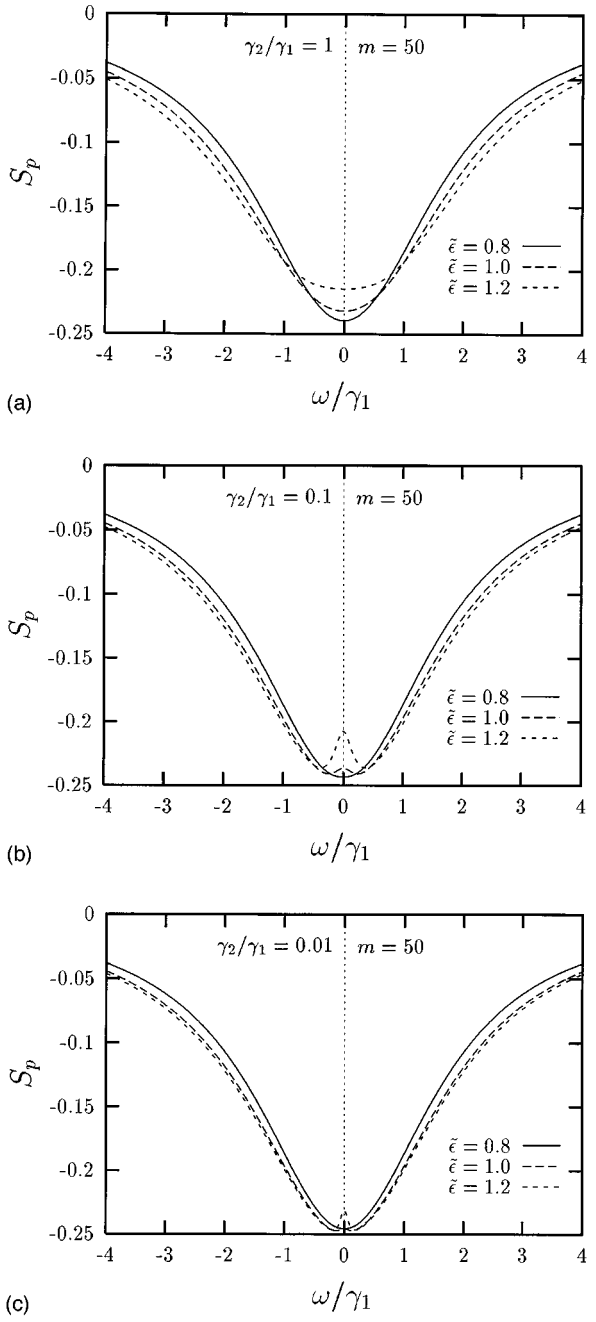

FIG. 15. Same as Fig. 14 for $m=50$.

this calculation and $\langle \tilde{a}_1 \rangle = 0$. (Since the width of the central dip scales with γ, it is not resolved for $\gamma=1$.)

B. Validity of mean-field and bare-vertex approach

In order to analyze the range of validity of the mean-field approximation and to understand the good agreement between mean-field and bare-vertex results for small values of γ, we estimate the self-energy contributions from both approximations. For this it is sufficient to compare the effective self-energy of the mean-field case, $K^2|\langle a_2 \rangle|^2 D^0_{11^+}$, with a representative bare-vertex correction P_{1^+1} for $\omega=0$. Substituting the mean-field results, we find

$$\frac{P^{-+}_{1^+1}(0)}{K^2|\langle a_2\rangle|^2 D^{0-+}_{11^+}(0)} = \frac{\gamma}{\gamma+(1-\langle \tilde{a}_2\rangle)} \frac{1}{4n_{\rm th}\gamma(1-\langle \tilde{a}_2\rangle)}. \tag{64}$$

Hence the one-loop corrections to the self-energy are small compared to the mean-field or Hartree terms, when the right-hand side (r.h.s.) of Eq. (64) is small compared to unity.

A similar condition has been found by Mertens *et al.* in Ref. [11] for the convergence of the Dyson equation. We here note, however, two essential differences: First Mertens *et al.* and also Plimak and Walls in [12] considered a case in which the effective decay rate of the subharmonic mode is smaller than that of the pump mode where the first factor on the r.h.s. of Eq. (64) is close to unity. Second, they approxi-

mated $\langle\tilde{a}_2\rangle$ in the denominator by the classical expression $\tilde{\epsilon}$. This second approximation, however, strongly underestimates the radius of convergence of the Green's function approach, since in the vicinity and above the classical threshold $\langle\tilde{a}_2\rangle$ deviates from $\tilde{\epsilon}$ substantially (compare Fig. 12). In particular, if we use mean-field results, we find in contrast to Mertens *et al.* that the second term in Eq. (64) never diverges,

$$\frac{P^{-+}_{1^+1}(0)}{K^2|\langle a_2\rangle|^2 D^{0-+}_{11^+}(0)} = \frac{\gamma}{\gamma+(1-\langle\tilde{a}_2\rangle)} 2(\tilde{\epsilon}-\langle\tilde{a}_2\rangle)$$

$$\approx \frac{\gamma}{\gamma+(1-\langle\tilde{a}_2\rangle)} 2(\tilde{\epsilon}-1) \qquad (65)$$

in the vicinity or above threshold. Thus an estimated upper limit for the pump rate up to which the mean-field approach is accurate is given by

$$\tilde{\epsilon}-1 \leqslant \frac{1}{2}\left[1+\frac{1-\langle\tilde{a}_2\rangle}{\gamma}\right]. \qquad (66)$$

We recognize that in the case opposite to that studied by Mertens *et al.* and Plimak and Walls, namely for a fast decaying subharmonic mode, such that $\gamma \ll (1-\langle\tilde{a}_2\rangle)$, the upper limit for the pump rate is considerably higher.

In order to test the validity of the bare-vertex approximation we now have to analyze under what conditions higher-order contributions to the self-energy are negligible. As pointed out by Mertens *et al.* [11], a consistent way of doing this is to take into account the first-order corrections in the vertex expansion of Γ, given in Eq. (50). Mertens *et al.* evaluated these contributions by replacing the exact Green's functions by the linearized expressions. This, however, considerably overestimates the two-loop contributions and does not allow one to test the approach at threshold. We use here the well-behaved expressions from the mean-field approach instead.

As an indicator of the reliability of the bare-vertex approximation we may use the quantity

$$\Delta P^{\text{eff}}_{\text{two-loop}} \equiv P^{\text{eff}}_{\text{two-loop}} - P^{\text{eff}}_{\text{one-loop}}, \qquad (67)$$

which is a 2×2 matrix in physical times. In order to obtain a single real number, we introduce the norm

$$||P|| \equiv \sqrt{P^{\alpha\beta}P^{\alpha\beta}}. \qquad (68)$$

Note that here again the Einstein notation applies. In Fig. 16 we have plotted the relative contributions of the two-loop terms to the effective self-energy for $\omega=0$,

$$q = ||\Delta P^{\text{eff}}_{\text{2-loop}}(\omega=0)||/||P^{\text{eff}}_{\text{1-loop}}(\omega=0)|| \qquad (69)$$

as a function of the pump parameter for $\gamma=0.1$ and different values of m. One recognizes that the bare-vertex approximation works well up to 20% above the classical threshold. For larger values of the pump strength it becomes unreliable in particular for larger system-size parameters m.

The breakdown of the vertex expansion above threshold can easily be understood. When the pump strength exceeds the critical value for the pitchfork bifurcation, the classical solutions become bistable. There is of course no bistable steady state in the quantum dynamics. However, the phase-space distribution of the subharmonic mode becomes double peaked. This situation is qualitatively different from the behavior below threshold, where the true state can be characterized by a Gaussian distribution around a well-defined classical amplitude. An approach based on semiclassical expansions must clearly break down in a bistable regime. However, if the system size is small, the transition from a single-peaked to a double-peaked distribution is smeared out and the bare-vertex approach works reasonably well also somewhat above the classical threshold.

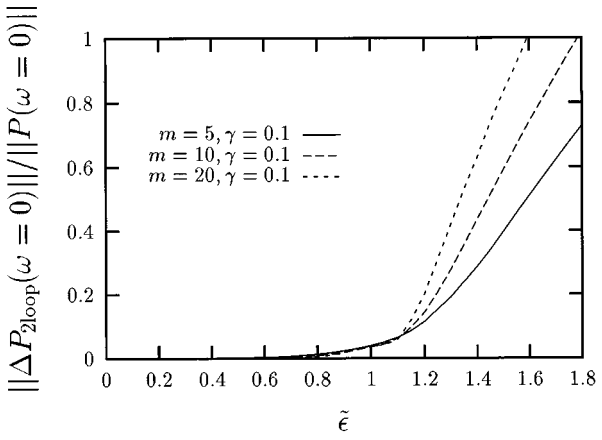

FIG. 16. Relative contribution of two-loop terms to self energies.

C. Bare-vertex approximation for the above-threshold OPO with symmetry breaking

From the preceding discussions it is clear that a semiclassical expansion fails to describe the true steady-state behavior of the parametric oscillator above threshold. However, since the tunneling time rapidly increases when one moves away from the threshold, there are two metastable states, with a mean subharmonic amplitude close to one of the bistable classical values. An external asymmetric perturbation can force the system into one of these states and it takes a long time before tunneling reestablishes the symmetric distribution. This property gives also the justification for a linearization around one of the two classical solutions above threshold [15]. Since the Green's-function approach does not include tunneling, it also corresponds to such a situation when applied to the above-threshold case with $\langle\tilde{a}_1\rangle \neq 0$.

In the present subsection we analayze the mean amplitudes and fluctuation spectra within the bare-vertex approximation above threshold lifting the restriction $\langle\tilde{a}_1\rangle=0$, which implies that also mixed-type Green's functions D_{12}, etc., need to be considered. Thus we need to resort to the general-case Dyson Equation (45) with self-energies given in Eq. (48). By using a nonvanishing value of $\langle\tilde{a}_1\rangle$ in the first step of iteration of the (now much more involved) Dyson equations we enforce a symmetry breaking. The true value of $\langle\tilde{a}_1\rangle$ in the (metastable or quasi)steady state then follows from the self-consistent iteration scheme.

In Fig. 17 we have plotted the mean amplitude of the subharmonic mode as a function of the pump strength for $m=5$ and $m=50$ and $\gamma=0.1$ and 1. For comparision also the classical solution is shown. One can recognize that for a larger system size of both modes ($m=50$, $n_{\text{th}}=25$) bare-

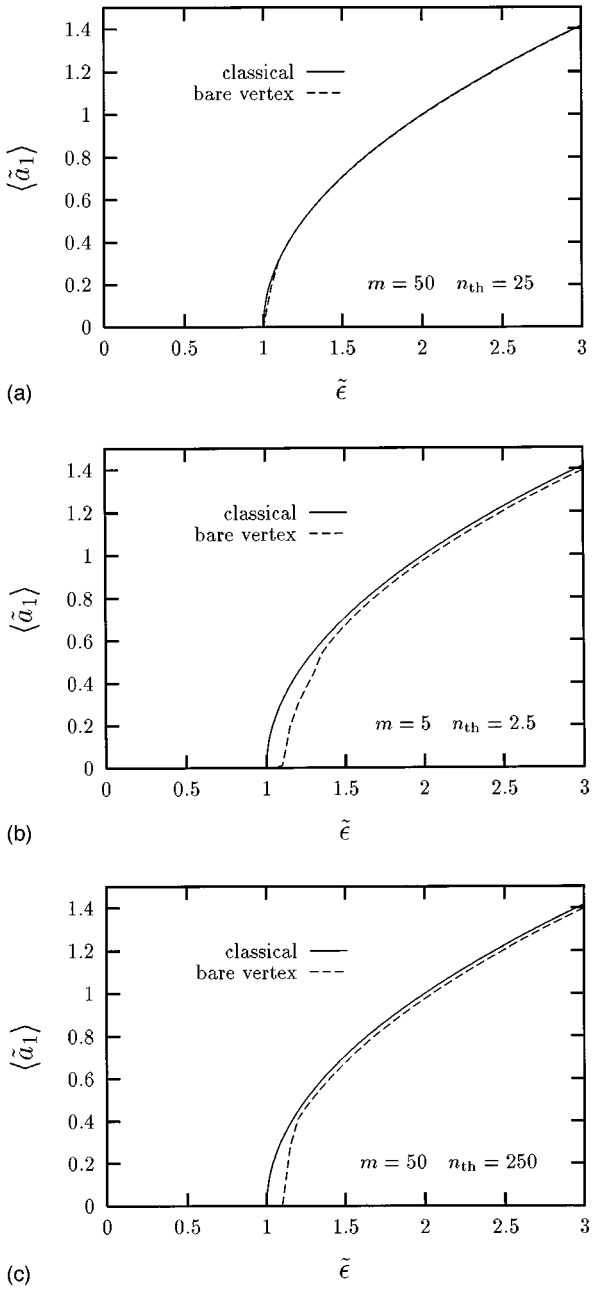

FIG. 17. Mean value of subharmonic amplitude in bare-vertex approximation with symmetry breaking for $n_{\rm th}=25$, $m=50$ ($\gamma=1$) shown in (a), for $n_{\rm th}=2.5$, $m=5$ ($\gamma=1$) shown in (b), and for $n_{\rm th}=250$, $m=50$ ($\gamma=0.1$) in (c).

vertex and classical solutions are virtually the same. For a smaller system size ($m=5$ and $n_{\rm th}=2.5$) or for a small value of $\gamma=\gamma_2/\gamma_1$ ($m=50$, $n_{\rm th}=250$, i.e., $\gamma=0.1$) the phase transition between $\langle \tilde{a}_1 \rangle = 0$ and $\langle \tilde{a}_1 \rangle \neq 0$ occurs at a substantially higher value of the pump rate. The point of the phase transition can be considered as renormalized threshold of parametric oscillation and finite-size effects shift this point towards a higher pump strength. It is interesting to note that for the range of the pump parameter shown, the mean value of the subharmonic mode stays below the classical value even for relatively large pump strength.

The squeezing spectrum above threshold shows the same features as known from linearization. It develops a peak

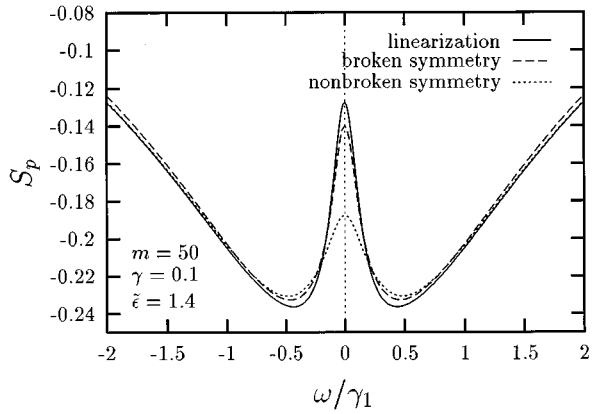

FIG. 18. Squeezing spectrum above classical threshold ($\tilde{\epsilon}=1.4$) from linearization, bare-vertex approach with and without symmetry breaking.

around $\omega=0$ which is narrower and more pronounced when γ is small. As can be seen from Fig. 18, finite size effects tend to smear out the sharp spectral structures. For comparison we have shown also the squeezing spectrum without symmetry breaking in Fig. 18, in which case the peak is much less pronounced. The antisqueezing spectrum is initially a Lorentzian which rapidly decreases in height with increasing pump strength until it becomes double peaked at frequencies $(\omega/\gamma_1)^2=(\omega_0/\gamma_1)^2=-\gamma^2+\gamma\sqrt{2\gamma|\langle\tilde{a}_1\rangle|^2+4|\langle\tilde{a}_1\rangle|^4}$ as in the linearization approach.

An interesting effect of the one-loop contributions to the fluctuation spectra above threshold was pointed out in Ref. [18]. Sufficiently far above threshold and for small values of γ additional small spectral peaks occur at frequencies $\omega=0$ and $\omega=\pm 2\omega_0$, where ω_0 is the peak-frequency in the linearized antisqueezed spectrum. For higher pump values these structures disappear again. We also find these structures in the antisqueezed spectrum as indicated in Fig. 19. The appearance of these peaks in a nonlinear theory is easily understood. As mentioned before, the fluctuations become spectrally condensed at frequencies $\pm\omega_0$ sufficiently far above threshold. The nonlinear terms in the equations of motion then result in beat-note terms at frequencies $\omega=0$ and $\pm 2\omega_0$. In the Dyson equations this effect is generated by the quadratic contributions in the self-energies. If we assume, for example, that $D^{\alpha\beta}_{1^+1^+}(\omega)$ has sharp peaks at $\omega=\pm\omega_0$, the

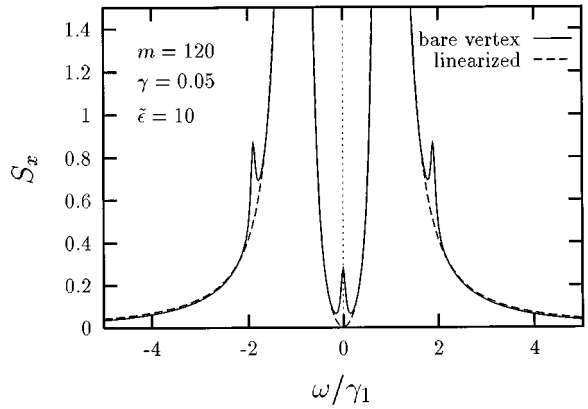

FIG. 19. Generation of beat-note contributions at $\omega=0$ and $\omega=\pm 2\omega_0$ in antisqueezing spectrum far above the classical threshold.

convolution integral in the one-loop contribution to the self-energy

$$P_{22}^{\alpha\beta}(\omega)=\frac{K^2}{4\pi}\alpha\beta\int d\omega' D_{1^+1^+}^{\alpha\beta}(\omega')D_{1^+1^+}^{\alpha\beta}(\omega-\omega') \tag{70}$$

leads to large contributions at $\omega=0$ and $\omega=\pm 2\omega_0$. When the pump strength is further increased, the absolute value of the fluctuations decreases and therefore the one-loop contributions to the self-energies become small compared to the mean-field terms. Thus the additional peaks in the fluctuation spectra disappear again.

V. SUMMARY

In the present paper we have analyzed the quantum statistical properties of a degenerate parametric oscillator with the help of a many-body approach. This approach does not make use of the small-noise assumption in linearization approaches and thus allows one to study the near-threshold behavior and effects from finite system sizes characterized by the two parameters m and n_{th}.

We have shown in Sec. II that the quantum dynamics of the parametric oscillator can be accurately described below, at, and to a certain degree above the classical threshold with a mean-field approach in the limit of a fast decaying subharmonic mode. The mean-field equations take into account the depletion of the pump mode due to energy transfer into subharmonic fluctuations, which is ignored in linearization approaches and can be solved analytically. The approach does require a large threshold photon number of the pump mode n_{th} in order for the pump mode to be treated quasiclassically but not a large system-size of the subharmonic mode. One can therefore study a semiquantum limit, with a highly quantum subharmonic mode. In this limit a large deviation not only of the fluctuations but also of the mean amplitudes of the fields from the linearization results can be found. As opposed to the linearization results, the intracavity antisqueezed fluctuations as well as the subharmonic photon number remain finite at threshold and scale with the square root of m.

Yielding well-behaved results for mean values and correlation functions, the mean-field approach is an appropriate starting point for more accurate approaches. Following the idea of Mertens, Kennedy, and Swain [9–11] we derived a closed set of Dyson equations for two-point Green's functions or field correlation functions in Sec. IV using the bare-vertex approximation. The Dyson equations are integral equations and are solved numerically by a self-consistent iteration scheme. As opposed to Mertens *et al.*, who used diverging linearized Green's functions for the initial self-energies, we used well-behaved mean-field values which are all-order expressions in $1/m$. In this way we were able to achieve convergence also at and above threshold.

In the first part of our analysis we assumed a vanishing mean amplitude of the subharmonic mode and studied the influence of finite-size effects on the squeezing in the threshold area. We found that with decreasing system size the amount of squeezing is generally reduced and the point of maximum intracavity fluctuations of the x component is shifted to pump strength larger than the threshold pump rate. Also the spectrum of squeezed fluctuations in the output is changed. For small values of γ, the double-peak structure known from linearization above threshold (with broken symmetry, i.e., $\langle\tilde{a}_1\rangle\neq 0$) appears already below threshold.

We have analyzed the range of validity of the bare-vertex approximation with vanishing subharmonic amplitude by estimating higher-order vertex corrections. For this, Green's functions from the mean-field approach were used as opposed to the analysis in Ref. [11], where linearized expressions were applied. We showed that the bare-vertex approximation works well at and to a certain degree above the classical threshold for small values of γ and small values of m. For higher pump strength the stationary phase-space distribution of the subharmonic mode becomes double peaked and the vertex expansion breaks down. The smaller the system size and the larger the decay of the subharmonic mode, the slower is the transition from the single to the double-peaked distribution and the longer the bare-vertex approach works.

In the second part of our analysis we studied the stationary OPO above the classical threshold relaxing the condition $\langle a_1\rangle=0$ and thus allowing for symmetry breaking. Since tunneling between the two classical stable states is not accounted for by the bare-vertex approach, this corresponds to an analysis of fluctuations in a metastable state. We showed that the critical pump strength for which a metastable state is possible is in general larger than the classical threshold value if the system size of the modes or the ratio of decay rates $\gamma=\gamma_2/\gamma_1$ are small. This can be considered as a renormalization of threshold due to finite-size effects.

In conclusion, the many-body technique is a useful tool to study quantum fluctuations beyond the level of linearization in particular finite-size effects whenever a well-defined single-peaked stationary phase-space distribution exists.

ACKNOWLEDGMENTS

The authors would like to thank T. A. B. Kennedy and C. Mertens for stimulating discussions and making Ref. [18] available prior to publication. O.V. thanks the Bayrisches Kultusministerium and the DAAD and M. F. the Alexander-von-Humboldt Stiftung for financial support.

[1] Ling An Wu, H. J. Kimble, J. L. Hall, and Huifa Wu, Phys. Rev. Lett. **57**, 2520 (1986); see also the special issues on ''squeezed light'': J. Opt. Soc. Am. B **4**, no. 10 (1987) and J. Mod. Opt. **37**, no. 6/7 (1987).

[2] M. J. Collett and D. F. Walls, Phys. Rev. A **32**, 2887 (1985); C. W. Gardiner, *Handbook of Stochastic Methods* (Springer, Berlin, 1985); C. W. Gardiner, *Quantum Noise* (Springer, Berlin, 1989).

[3] R. Schack and A. Schenzle, Phys. Rev. A **41**, 3847 (1990); F. Kärtner, R. Schack, and A. Schenzle, J. Mod. Opt. **39**, 917 (1992).
[4] P. D. Drummond, K. J. McNeil, and D. F. Walls, Opt. Acta **28**, 211 (1981).
[5] G. J. Milburn and D. F. Walls, Opt. Commun. **39**, 401 (1981).
[6] L. A. Lugiato and G. Strini, Opt. Commun. **41**, 67 (1982).
[7] M. Wolinsky and H. J. Carmichael, Phys. Rev. Lett. **60**, 1836 (1988).
[8] P. Kinsler and P. D. Drummond, Phys. Rev. A **52**, 783 (1995).
[9] C. J. Mertens, T. A. B. Kennedy, and S. Swain, Phys. Rev. Lett. **71**, 2014 (1993).
[10] C. J. Mertens, T. A. B. Kennedy, and S. Swain, Phys. Rev. A **48**, 2374 (1993).
[11] C. J. Mertens, J. Hasty, H. H. Roark III, D. Nowakowski, and T. A. B. Kennedy, Phys. Rev. A **52**, 742 (1995).
[12] L. I. Plimak and D. F. Walls, Phys. Rev. A **50**, 2627 (1994).
[13] O. Veits and M. Fleischhauer, Phys. Rev. A **52**, 4344 (1995).
[14] See, for example, L. P. Kadanoff and G. Baym, *Quantum Statistical Mechanics* (Benjamin, New York, 1962); V. Bonch-Bruevich and S. Tjablikov, *The Green's Function Method in Statistical Mechanics* (North Holland, Amsterdam, 1962); A. L Fetter and J. D. Walecka, *Quantum Theory of Many-Particle Systems* (McGraw Hill, New York, 1971); D. J. Amit, *Field Theory, the Renormalization Group and Critical Phenomena* (World Scientific, Singapore, 1984).
[15] M. J. Collett and D. F. Walls, Phys. Rev. A **32**, 2887 (1985).
[16] R. J. Glauber, Phys. Rev. Lett. **10**, 84 (1963); P. L. Kelley and W. H. Kleiner, Phys. Rev. **136**, A316 (1964).
[17] L. V. Keldysh, Zh. Éksp. Teor. Fiz. **47**, 1515 (1964) [Sov. Phys. JETP **20**, 1018 (1965)].
[18] C. J. Mertens and T. A. B. Kennedy, Phys. Rev. A **53**, 3497 (1996).